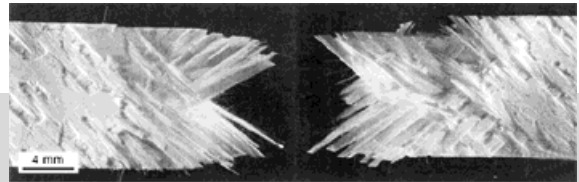


# Mechanical Properties of Porous-Matrix Ceramic Composites\*\*

By Frank W. Zok\* and Carlos G. Levi

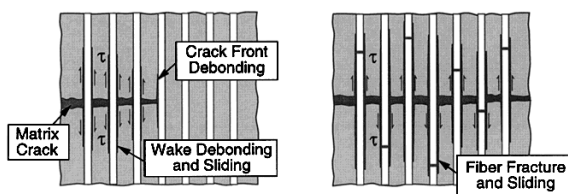


The use of porous matrices to enable damage tolerance in ceramic composites has emerged as a new paradigm in high performance materials. This paradigm obviates the need for fiber coatings for the purpose of crack deflection, thereby providing opportunities for lower cost manufacturing relative to that of conventional coated-fiber systems. Furthermore, upon selection of all-oxide constituents, the prospect for meeting the long-term durability requirements of high-temperature components for future gas turbine engine technologies becomes realizable. This article reviews the mechanical properties of this class of all-oxide composite. The properties of interest include the in-plane strength and notch-sensitivity subject to both fiber- and matrix-dominated loadings, and interlaminar strength. Special emphasis is placed on the role of the porous matrix in each of these properties. Finally, the issue of the stability of the matrix microstructure following prolonged exposure at elevated temperature is addressed and its role in maintaining desirable mechanical properties is demonstrated.

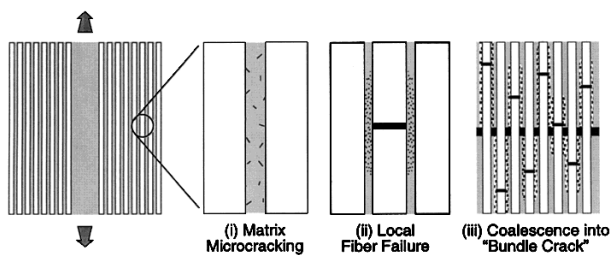
## 1. Introduction

Damage tolerance can be enabled in continuous fiber-reinforced ceramic composites (CFCCs) in one of two ways. The more conventional approach involves the use of fiber coatings to promote crack deflection and frictional sliding along the fiber-matrix interfaces<sup>[1]</sup> (Fig. 1a). These mechanisms per-

mit the development of multiple matrix cracks, which in turn produce inelastic strain during tensile loading. Furthermore, they provide a means for mechanically decoupling the fibers from one another and hence allow the fibers to fail in an uncorrelated manner. The latter feature has important implications in the attainment of a high fiber bundle strength and energy dissipation during pullout of broken fibers. The second approach involves the use of a controlled amount of fine-scale matrix porosity, obviating the need for a fiber coating (Fig. 1b). This approach can be viewed as an extension of the porous coating concept wherein crack deflection occurs because of the low fracture toughness of the porous interphase.<sup>[1-3]</sup>



(a) Conventional (Weak Interface) Concept



(b) Porous Matrix Concept

Fig. 1. Schematics of the damage processes that enable damage tolerance in a) conventional dense-matrix weak-interface CFCCs and b) porous matrix CFCCs without fiber coatings.

[\*] Prof. F. W. Zok, Prof. C. G. Levi  
High Performance Composites Center  
Materials Department  
University of California  
Santa Barbara, CA 93106-5050 (USA)  
E-mail: zok@engineering.ucsb.edu

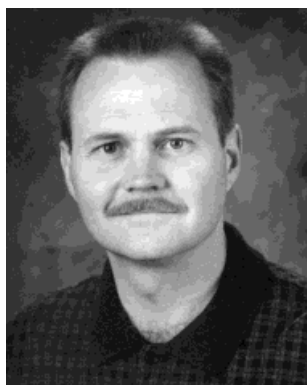
[\*\*] The research on oxide composites at UCSB is currently sponsored by the Air Force Office of Scientific Research under Contract No. F49620-99-1-0259, monitored by Dr. Thomas Hahn. The authors would like to thank Eric Carelli, Thomas Mackin, Michael Mattoni, Mark Roberts, and James Yang for their contributions to this review.

The porous matrix concept has been developed primarily in the context of oxide-based composites. This development can be attributed to two factors. The first relates to the ability to produce a controlled pore structure in the matrix at temperatures below that wherein the fiber properties begin to degrade. This is accomplished either by partially sintering a network of fine particulate or by pyrolysis of a ceramic precursor, both of which are generally more amenable to oxide constituents than to carbides or nitrides. The second factor is the shortage of robust fiber coatings available for use with oxide fibers. Such coatings must satisfy a number of requirements, including thermochemical compatibility with the fibers, oxidation resistance at elevated temperature, low toughness, and moderate processing temperature. A number of oxide coatings with some of the requisite properties have been developed recently, including monazite,<sup>[4-6]</sup> scheelite,<sup>[7]</sup> and hibonite.<sup>[8,9]</sup> The coatings are typically applied by immersing the fibers into either a ceramic slurry or a ceramic precursor solution of the coating material, followed by an elevated temperature treatment to effect pyrolysis and/or densification of the coating material. Despite this progress, there remain barriers in the implementation of these coatings in a large-scale production environment. One of the key problems is the application of the coatings uniformly over the fiber surfaces while keeping the fibers separated, especially once the fibers are woven into a fabric.

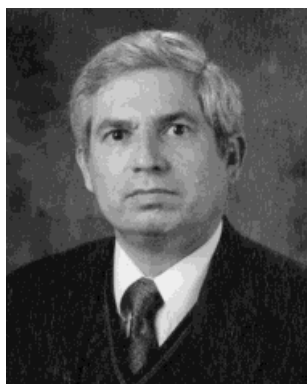
Although the porous matrix concept offers new opportunities for the development of damage tolerant CFCCs, it also poses new challenges in the design and synthesis of micro-

structures that meet the opposing property requirements placed on the matrix. In the absence of fiber coatings, the matrix must be sufficiently weak to enable damage tolerance under fiber-dominated loadings, yet retain adequate strength to ensure acceptable off-axis properties. In principle, the combination of properties can be tailored through changes in the state of the matrix. For instance, improvements in the interlaminar strength and off-axis in-plane strength can be obtained by reducing the matrix porosity, but these come at the expense of a reduction in the damage tolerance under fiber-dominated loadings.<sup>[10]</sup> These offsetting effects suggest the existence of an optimum in the matrix properties at which an appropriate balance of properties is achieved. However, the connections between matrix structure and composite performance are understood presently at only a rudimentary level. Consequently, the pathway to optimization remains ill defined.

The present article provides an overview of the mechanical properties of porous-matrix composites, with emphasis on connections between properties and matrix microstructure. The article is organized in the following way. The basic concepts underlying damage tolerance in porous matrix CFCCs in the absence of fiber coatings are reviewed in Section 2. Section 3 describes the constituent materials that are currently of interest, mainly for use in CFCCs for thermostructural applications (e.g., gas turbine components). The subsequent sections focus on various property groups. Within each, the phenomenology of the deformation and/or failure mechanisms and typical values of the relevant material properties are pre-



*Frank Zok obtained his Ph.D. degree from McMaster University, Canada, in Materials Engineering in 1988. He joined the faculty at the University of California at Santa Barbara in 1990 and is presently Professor in the Materials Department. His research interests concern the thermal and mechanical behavior of structural composite materials. He is Associate Editor for the Journal of the American Ceramics Society and is the author of approximately 100 scientific papers.*



*Carlos G. Levi received a Ph.D. in Metallurgical Engineering from the University of Illinois at Urbana-Champaign in 1981. He joined the faculty at the University of California, Santa Barbara, in 1984 and is presently Professor of Materials and Mechanical Engineering. His research emphasizes the understanding of microstructure evolution during synthesis and processing, and the application of this understanding to the design and manufacture of improved materials. He is a former recipient of the Howe Medal and Grossman Awards from ASM International, currently serves as Vice-Chair of the Materials Processing and Manufacturing Division at TMS, and is a member of the Editorial Board of Materials Science and Engineering. He has published approximately 100 scientific papers.*

sented. The basic mechanical properties, including in-plane tensile behavior and interlaminar strength, are described in Section 4. Issues regarding notch sensitivity are addressed in Section 5. Finally, the role of matrix densification during high temperature exposure in composite performance is demonstrated in Section 6.

## 2. Matrix-Enabled Damage Tolerance

Broadly, damage tolerance in CFCCs is obtained when the matrix acts as a mechanical “buffer” between adjacent fibers, essentially isolating the fibers from one another. To this end, cracks in the matrix must not penetrate into the fibers. Similarly, fiber breaks must remain isolated and induce minimal stress concentration in neighboring fibers. A secondary consideration involves the resistance to shear deformation within the matrix, especially as it relates to the local deformation and stress concentration in the region surrounding a fiber break. Transfer of load from a broken fiber to the surrounding matrix and fibers via shear deformation can increase the load bearing capacity of the composite as well as enhance the fracture energy. However, there is an optimum in the matrix strength beyond which the load transfer between fibers becomes excessively localized and the fiber damage spreads in a correlated manner with attendant reductions in strength and damage tolerance. The sequence of damage events leading to composite fracture under tensile loading parallel to the fiber direction is illustrated in Figure 1b.

Some insights into the conditions that satisfy these requirements are obtained from the mechanics of cracks at an interphase boundary.<sup>[11]</sup> Figure 2 shows some of the key features. As a minimum condition for damage tolerance, cracks in the matrix must either arrest at or deflect into the fiber/matrix interface. The conditions for deflection are determined by considering the two energy release rates,  $G_p$  and  $G_d$ , associated with penetration across the interphase boundary and deflection into the boundary, respectively. The key material property dictating the ratio  $G_d/G_p$  is the elastic mismatch parameter:  $\alpha \equiv (\bar{E}_f - \bar{E}_m)/(\bar{E}_f + \bar{E}_m)$  where  $\bar{E}$  is the plane strain

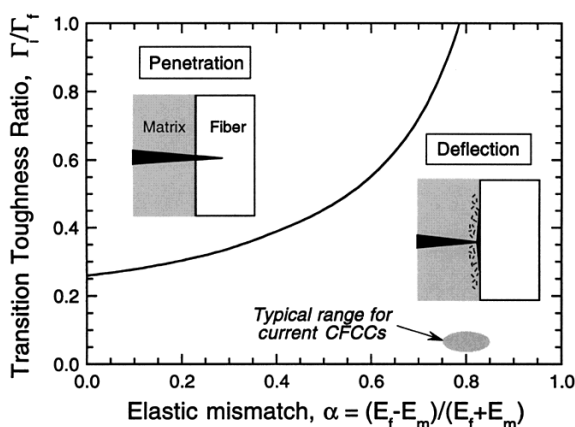


Fig. 2. Interactions of cracks with interphase boundaries in porous-matrix CFCCs. The shaded regions denote the matrix and the white regions denote the fiber.

modulus, and the subscripts f and m refer to the fiber and matrix, respectively. At the simplest level, the effect of matrix porosity on the modulus can be described by an empirical relationship of the form:<sup>[12]</sup>

$$E_m/E_m^0 = 1 - (p_m/p_0) \quad (1)$$

where  $E_m$  and  $E_m^0$  are the moduli of the porous and fully-dense matrices,  $p_m$  is the matrix porosity, and  $p_0$  is the initial matrix porosity (following slurry infiltration). Typically,  $p_m/p_0 \approx 0.9$  and hence  $E_m/E_m^0 \approx 0.1$ . Furthermore, taking  $E_f/E_m^0 \approx 1$  yields an elastic mismatch  $\alpha \approx 0.8$ .

The additional critical parameter in the determination of the deflection condition is the ratio,  $\Gamma_i/\Gamma_f$ , where  $\Gamma_i$  and  $\Gamma_f$  are the toughnesses (in units of  $J m^{-2}$ ) of the fiber–matrix interface and the fibers, respectively. In the absence of a fiber coating, the interface toughness is expected to be no greater than that of the porous matrix,  $\Gamma_m$ , a consequence of the reduced efficiency of particle packing along the fiber surface. To obtain a conservative estimate of the conditions needed to prevent crack penetration, the matrix and interface toughnesses are taken to be equal to one another ( $\Gamma_i = \Gamma_m$ ). In turn, the toughness of the matrix can be related to its porosity content using a simple linear relation, similar to that used for the modulus:<sup>[12]</sup>

$$\Gamma_m/\Gamma_m^0 = 1 - (p_m/p_0) \quad (2)$$

where  $\Gamma_m^0$  is the toughness of the fully dense matrix. Again, for  $p_m/p_0 \approx 0.9$ ,  $\Gamma_m/\Gamma_m^0 \approx 0.1$ . Upon inspection of Figure 2, it is evident that this combination of elastic mismatch and toughness ratio satisfies the conditions for the deflection of matrix cracks into the interface. This prediction is consistent with the observation that pre-existing matrix cracks (introduced during processing, e.g., Fig. 3) have no apparent effect on the fiber-dominated properties.<sup>[13,14]</sup> Furthermore,

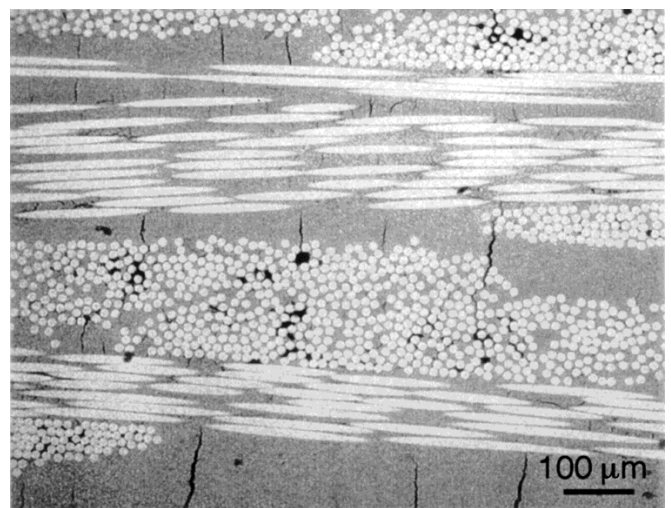


Fig. 3. Scanning electron micrograph of a porous-matrix CFCC showing processing cracks within the matrix (backscatter electron imaging mode). (Courtesy J.-Y. Yang, University of California at Santa Barbara).

the figure reveals a significant “gap” between the critical condition for crack penetration into the fibers and the conditions obtained in current generations of porous-matrix CFCCs. This suggests that the matrix porosity could be reduced further, for the purpose of enhancing the off-axis properties, yet still satisfy the crack deflection condition.

Once the fibers begin to fail, the subsequent behavior is dictated by the nature and extent of inelastic deformation within the surrounding matrix and the effect of this deformation on the stress concentration in neighboring fibers. In this context, the relevant matrix property is its “yield strength”; the mechanism of yield and subsequent inelastic straining involves fracture of the necks between particles and subsequent rearrangement of the particles (analogous to flow of granular materials). Quantitative connections between the macroscopic yield and flow properties and the chemistry and topology of the matrices have yet to be established. Nevertheless, experience with other fiber composites, including weakly-bonded ceramic composites as well as strongly bonded metal- and polymer-matrix composites, provides insights into the expected behavior of the porous-matrix CFCCs. For instance, when the matrix is sufficiently weak, the stress concentrations around fiber breaks remain small and, consequently, the fibers fail in a stochastically random manner.<sup>[15]</sup> Conversely, when the matrix is strong, stress concentrations develop and fiber failure spreads in a correlated manner, with each successive break being more likely to occur in the vicinity of an existing break or cluster of breaks.<sup>[16]</sup> A consequence is that the in-situ fiber bundle strength is intrinsically stochastic. Furthermore, the mean fiber bundle strength is reduced.

The expected correlations between the fiber bundle strength, composite damage tolerance, and matrix strength have been largely confirmed through experiments on a family of porous-matrix CFCCs with varying levels of matrix porosity.<sup>[10]</sup> When the matrix is highly porous ( $\approx 35\text{--}40\%$ ), the fracture surface exhibits extensive fiber “pullout”, consistent with random fiber failure (Fig. 4a). In this case, the strength and fracture toughness are high. Upon increasing the matrix density, the fiber failure sites become more correlated with one another, as manifest in planar fracture surfaces (Fig. 4b). Concomitantly, both the strength and fracture toughness of the composite decrease dramatically.<sup>[10]</sup>

### 3. Materials

The majority of composites produced to date employ one of the Nextel oxide fibers (3M Corporation) as the reinforcement. Among these, preference has been given to Nextel 610 because of its high strength at low and moderately high temperatures (to  $\sim 1000^\circ\text{C}$ ), and to Nextel 720 for its good creep resistance up to temperatures of  $\sim 1200^\circ\text{C}$ . In all cases of practical interest, the fibers are in the form of two-dimensional fabric in an 8-harness satin weave.

The matrices are typically mixtures of either alumina and silica,<sup>[17–20]</sup> or mullite and alumina.<sup>[10,13,14,21]</sup> The former is typical-

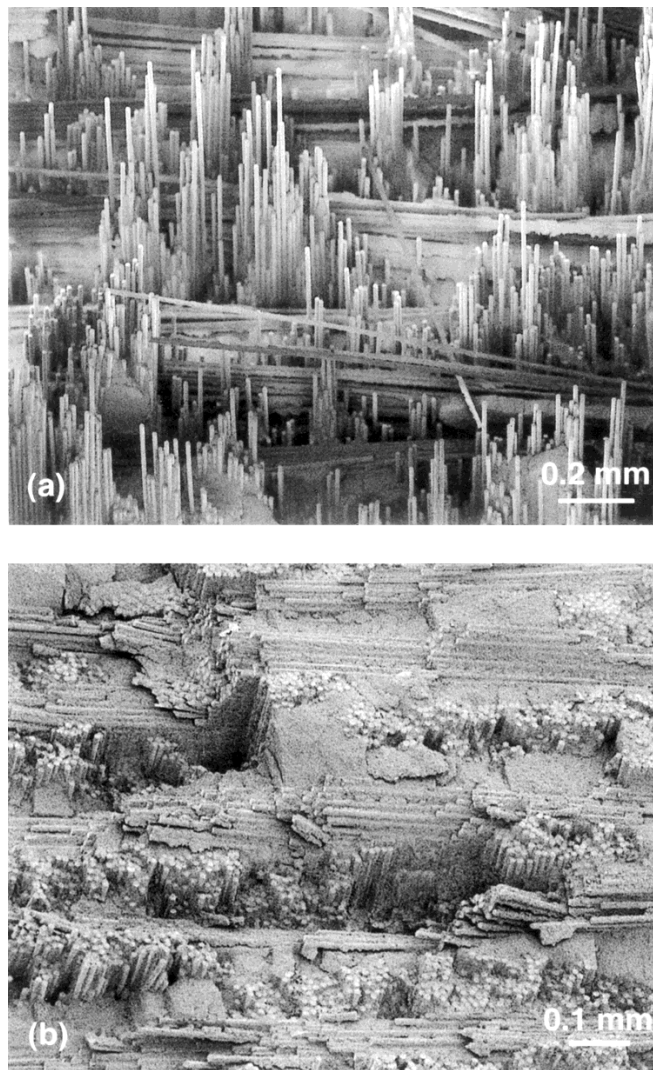


Fig. 4. Fracture surfaces of porous matrix CFCCs, showing a) un-correlated and b) correlated fiber fractures in CFCCs with weak and strong matrices, respectively. (Courtesy Michael Mattoni, University of California at Santa Barbara).

ly incorporated by immersing the fabric into a slurry containing alumina particulate and a silica-forming polymer, thereby producing a pre-preg that is subsequently used for component fabrication following established lay-up, curing, pyrolysis and sintering operations. When complete, this process yields a contiguous nanoporous silica phase within the alumina particle network. The mullite–alumina matrix is typically produced through pressure-assisted infiltration of a slurry with the appropriate composition and rheology into a fiber pre-form,<sup>[13,22]</sup> followed by drying and sintering. (Vibration-assisted intrusion of a consolidated wet matrix has also been demonstrated.<sup>[23]</sup>) The process can be augmented by subsequent impregnation and pyrolysis of a ceramic precursor in order to increase the structural integrity of the matrix. An alternate approach to bond a particle network by evaporation–condensation in reactive atmospheres has also been explored.<sup>[23]</sup>

The resultant matrix is characterized by a network of bonded particulate and a contiguous pore structure with a

size scale comparable to the particle size ( $\leq 1 \mu\text{m}$ ). The porosity levels required to enable damage tolerance typically fall in the range of  $\approx 30\text{--}40\%$ .<sup>[10,21]</sup> Stability of this pore structure in service is essential to the long-term preservation of the damage tolerant properties. For this reason, the major phase in these matrices should ideally form a contiguous network that inhibits shrinkage at elevated temperature, thereby providing stability to the pore structure, whereas the minor phase serves as a binder to impart mechanical strength.<sup>[14]</sup> In this context, mullite is preferred over alumina as the major phase because it exhibits more sluggish sintering kinetics and is therefore more resistant to shrinkage upon prolonged exposure to elevated temperatures.<sup>[13,14]</sup>

In practical situations, there is always some shrinkage associated with drying, pyrolysis and sintering (depending on the matrix), leading to the formation of matrix cracks predominantly normal to the fiber directions, such as those shown in Figure 3. Similar cracks are obtained in most C- and SiC-fiber reinforced C-matrix composites.<sup>[24,25]</sup> However, these cracks do not appear to be particularly detrimental to the important mechanical properties of the composite.<sup>[14,21]</sup> This result supports the notion that matrix cracks do not penetrate into the fibers, as described in the preceding section.

#### 4. Basic Mechanical Properties

In composites with 2-dimensional cross-ply fiber architectures, the basic in-plane mechanical properties are obtained from uniaxial tensile tests both along the fiber axis (in the  $0^\circ/90^\circ$  orientation) and an angle of  $45^\circ$ . The two test configurations provide the requisite information on the fiber-dominated and matrix-dominated properties, respectively. Additional information required for mechanical design involves the interlaminar properties, measured in shear and/or tension. The general mechanical characteristics and typical property values obtained from such tests are summarized below.

In the  $0^\circ/90^\circ$  orientation, the tensile response is characterized by nearly linear behavior up to fracture (Fig. 5). The

absence of more pronounced non-linearity is attributable to the high matrix porosity and the correspondingly low matrix stiffness. That is, since the matrix contribution to the initial composite stiffness is small, reductions in stiffness due to matrix damage are similarly small. Indeed, the Young's modulus of the porous mullite-alumina matrix is only  $\approx 20\text{--}25 \text{ GPa}$ :<sup>[21]</sup> about an order of magnitude less than that of the Nextel fibers. The absence of non-linearity may also be due in part to the presence of the pre-existing matrix cracks, which have the effect of further reducing the matrix contribution to the composite stiffness. This behavior is similar to that of C- or SiC-fiber reinforced C-matrix composites, which also exhibit nearly linear tensile behavior because of a combination of a low matrix modulus and extensive processing-derived matrix cracks. Provided the porosity level is sufficiently high, the fracture surface exhibits a fibrous appearance, a manifestation of the fiber failure events being largely un-correlated with one another (Fig. 4a). This feature demonstrates the efficacy of the porous matrix in de-coupling the fibers from one another. The composite properties are largely dictated by the type of fiber used for reinforcement. For fiber contents,  $f$ , in the range  $35\text{--}40\%$ , typical property values are: i) Young's modulus,  $E \approx 60\text{--}110 \text{ GPa}$ , and ii) ultimate strength,  $\sigma_u \approx 140\text{--}220 \text{ MPa}$ ,<sup>[13,17,21]</sup> the higher values are characteristic of Nextel 610 and the lower ones are characteristic of Nextel 720.

In the  $\pm 45^\circ$  orientation, the composite exhibits lower elastic modulus and ultimate tensile strength than the corresponding values in the  $0^\circ/90^\circ$  orientation, but a greater capacity for inelastic straining (Fig. 5).<sup>[20,21]</sup> Furthermore, the tensile strength is dictated by the formation of a diffuse localized deformation band, analogous to necking in metals.<sup>[21]</sup> Following localization, substantial amounts of additional remote displacement are obtained without fracture because of the straining within the localized band. Within this band, the deformation is accommodated by rotation of the fiber tows towards the loading direction through a "scissoring" action and comminution of the intervening matrix (Fig. 6). The spa-

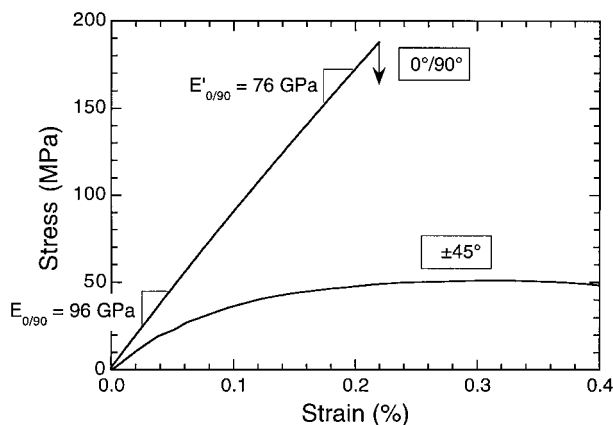


Fig. 5. Typical tensile properties of a porous-matrix CFCC in both  $0^\circ/90^\circ$  and  $\pm 45^\circ$  orientations. The material comprises Nextel 610 fibers in an 8-harness satin weave and a matrix of  $\approx 80\%$  mullite and  $20\%$  alumina [13,21]. Virtually the same behavior is obtained in CFCCs with matrices of alumina and silica [17,20].

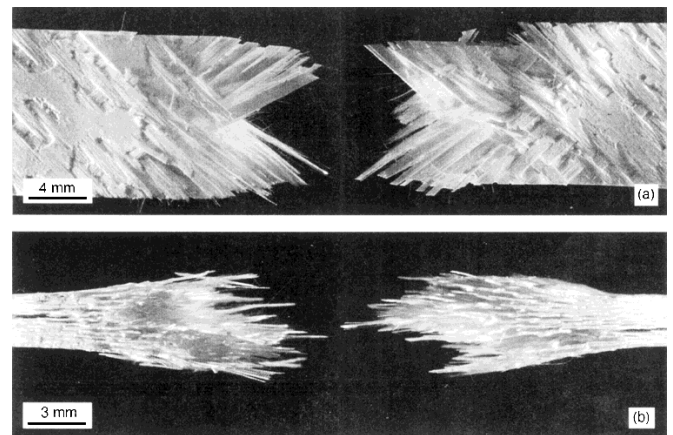


Fig. 6. Two orthogonal views of a fractured tensile specimen in the  $\pm 45^\circ$  orientation, showing a) fiber "scissoring" within the plane of the fabric, and b) swelling in the through-thickness direction, a consequence of comminution of the matrix during deformation [13].

tial extent of the localization and hence the amount of energy dissipated beyond localization are proportional to the specimen width (Fig. 7).<sup>[21]</sup> It is surmised that the tensile strength and failure strain would be greater in geometries where the localization is suppressed, such as cylindrical tubes with  $\pm 45^\circ$  fiber architectures. Typical property values for composites in the  $\pm 45^\circ$  orientation with mullite-alumina or alumina-silica matrices are: i) Young's modulus  $\approx 45\text{--}50$  GPa, ii) tensile strength  $\approx 50\text{--}60$  MPa, and iii) failure strain (at the onset of localization)  $\approx 0.2\text{--}0.4\%$ .<sup>[13,20,21]</sup> Since these properties are largely dominated by the matrix, they are insensitive to the fiber type.

The interlaminar shear strength (ILSS) is obtained either by short beam shear tests or by double-notched compression tests. In the porous matrix composites, the strengths fall in the range 8–12 MPa, increasing slightly with decreasing matrix porosity.<sup>[10,13,20]</sup> Furthermore, in the alumina/silica matrix systems, the ILSS increases with temperature, to  $\approx 20$  MPa at  $1000^\circ\text{C}$ .<sup>[20]</sup> This increase appears to be due to softening of the aluminosilicate phase and the resulting increase in matrix toughness. Under through-thickness tensile loading, the strengths are lower, in the range 3–7 MPa.<sup>[17]</sup> By comparison, the through-thickness tensile strengths of conventional dense-matrix weak-interface composites are  $\sim 10$  MPa,<sup>[17]</sup> a consequence of the higher matrix density and hence higher matrix strength. The relatively low interlaminar strengths of the porous matrix CFCCs remains a concern in their implementation in structural applications.

### 5. Notch Sensitivity

Notch sensitivity is most conveniently assessed through tensile tests on specimens containing a center hole, a center notch, or edge notches. The trends in the strength of center-hole specimens in the  $0^\circ/90^\circ$  orientation are plotted in Fig. 8. Two important features emerge. First, the net-section strength decreases with increasing hole size for self-similar geometries.<sup>[13,21]</sup> This trend indicates a size scale-dependence in the failure condition. Additional evidence of scale-dependence is

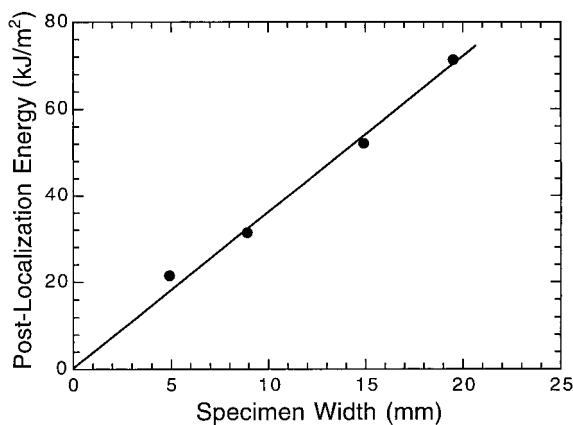


Fig. 7. Effects of specimen width on the energy absorption capacity following the onset of strain localization in the  $\pm 45^\circ$  orientation. (Adapted from [21].)

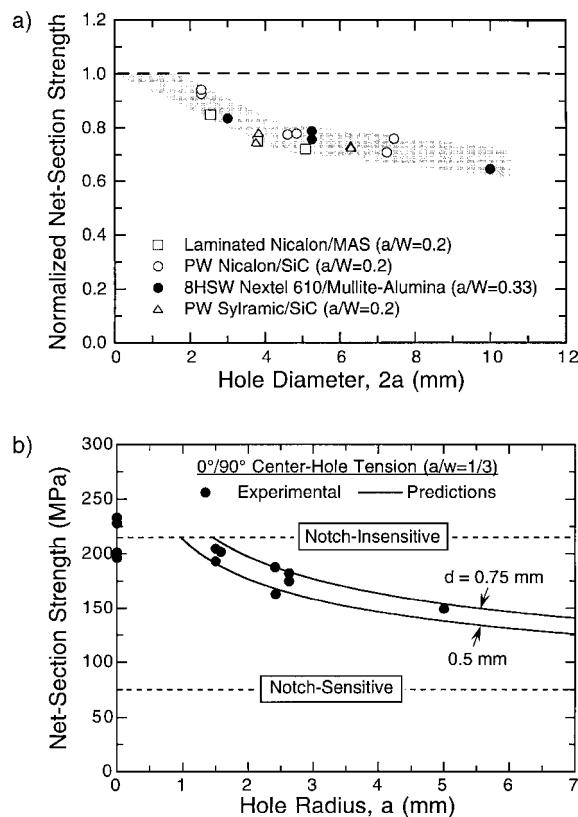


Fig. 8. Notch sensitivity of porous matrix CFCCs in the  $0^\circ/90^\circ$  orientation: a) normalized notched strength, with comparisons to conventional dense-matrix weak-interface systems, and b) comparisons with predictions based on the point stress failure criterion. PW: Plain weave; 8HSW: eight harness satin weave. (Adapted from [13] and [21].)

obtained from comparisons of the failure strains obtained locally ahead of the hole and in un-notched tensile specimens, the former being substantially greater than the latter. Similar conclusions are drawn from comparisons of the failure strains measured in bending and in tension.<sup>[21]</sup> Secondly, the trend in normalized strength is essentially the same as that of the conventional weak-interface systems. Both exhibit some reduction in strength, but substantially less than that predicted on the basis of elasticity. This difference is attributable to the inelastic straining that occurs ahead of the hole and its effect on mitigating stress concentrations. Furthermore, the similarity in the magnitude of the normalized strengths in the two classes of CFCCs demonstrates the efficacy of the porous matrix in enabling damage tolerance. Similar conclusions regarding notch insensitivity have been obtained from tests on double edge-notched specimens with notches of various root radii and stress concentrations ranging from 1 to  $\sim 8$ .<sup>[19]</sup>

Additional insight is obtained from in-situ measurements of stresses in notched specimens using a thermoelastic technique.<sup>[26]</sup> (The technique involves cyclic loading at a moderately high frequency,  $\sim 10$  Hz, and measurement of the in-phase periodic temperature change using an infrared imaging system.) Figure 9 shows a pair of representative images of a double-notched tensile specimen, at both low and moderately high levels of applied stress. Comparison of the images shows a reduction in the "hot spot" ahead of the

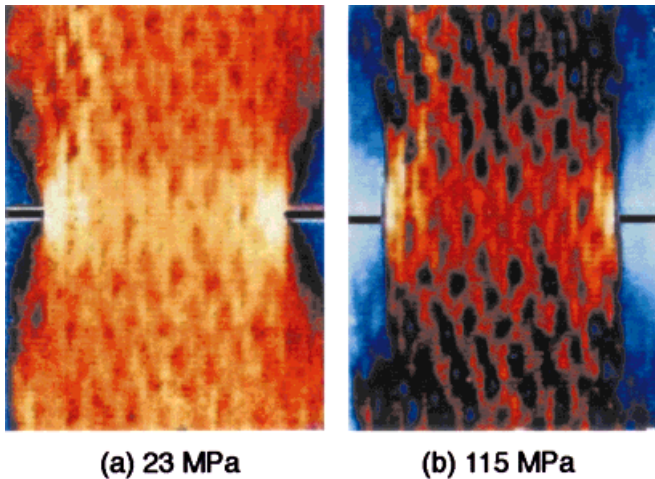


Fig. 9. Thermoelastic images of a double edge-notched specimen of a porous matrix CFCC at applied stress levels of a) 17 MPa and b) 86 MPa. (Courtesy Thomas Mackin and Mark Roberts, University of Illinois at Urbana Champagne.)

notch at the higher stress level coupled with an expansion of the low-stress wake region adjacent to the notches. The images further indicate that inelastic straining occurs in shear, nominally parallel to the loading direction, similar to that in C-matrix composites.<sup>[24]</sup> The inelastic deformation is essential to the mitigation of the notch tip stress concentration and the absence of severe notch sensitivity.

The effects of inelastic deformation on the stress and strain distributions around notches and holes have been determined from finite element calculations using a nonlinear constitutive law appropriate to CFCCs.<sup>[21]</sup> The law is calibrated using un-notched tension and shear data. The response in other orientations, subject to arbitrary bi-axial loads, is predicted by the model. Comparisons of the predictions with the experimental measurements reveal that the local tensile stresses and strains can exceed by a significant amount the values at fracture measured in uni-axial tension on standardized test coupons, providing further evidence of size-scale effects on strength. One approach that has found utility in rationalizing this effect comprises the point stress failure criterion. Here, fracture is postulated to initiate when a critical stress (usually taken to be the un-notched strength) is attained over a characteristic length,  $d$ , ahead of the notch. Upon combining this failure criterion with the calculated stress distributions, the characteristic length is inferred. Some typical results are plotted in Figure 8b for  $d = 0.5$  and  $0.75$  mm. The calculated results are in good agreement with the experimental measurements. Moreover, the inferred values of the characteristic distance in the porous matrix CFCCs are virtually identical to those obtained on the dense-matrix weak-interface systems.<sup>[27]</sup>

One limit to the notch sensitivity is obtained when small-scale yielding conditions prevail, i.e., the spatial extent of the nonlinear deformation is confined to a small volume surrounding the tip of a growing crack. In this limit, linear elastic fracture mechanics (LEFM) applies. The relevant material property is the steady-state fracture resistance, expressed in

terms of either a critical stress intensity factor,  $K_{ss}$ , or toughness,  $G_{ss}$ . The latter quantity can be estimated from the work of fracture of a notched bend specimen, provided the load-displacement response is continuous and does not exhibit precipitous load drops associated with sudden bursts of crack growth. Figure 10 shows a desirable curve for a composite with Nextel 610 fibers and a mullite-alumina matrix. The toughness is  $G_{ss} \approx 6000$  J/m<sup>2</sup> and the corresponding critical stress intensity factor is  $K_{ss} = \sqrt{EG_{ss}} \approx 25$  MPa m<sup>1/2</sup>: comparable to the values of high strength Al alloys. However, these values are not realized in the CFCCs under large scale yielding conditions, which arise when either the notch length or specimen width are small. Large-scale yielding models predict that steady state behavior is only obtained when these dimensions exceed a characteristic value, defined by  $a_c \approx \alpha EG_{ss} / \sigma_u^2$ , where  $\sigma_u$  is the un-notched strength and  $\alpha$  is a numerical coefficient of order 2. Using the material properties pertinent to the Nextel 610/mullite-alumina CFCC, the characteristic length is predicted to be  $a_c \approx 30$  mm. This length is considerably greater than the notch dimensions used in most material characterization studies. Consequently, LEFM is not expected to apply to the regime covered by the available measurements.

In the  $\pm 45^\circ$  orientation, the tensile strength is unaffected by the presence of circular holes, up to hole diameters of  $\sim 6$  mm

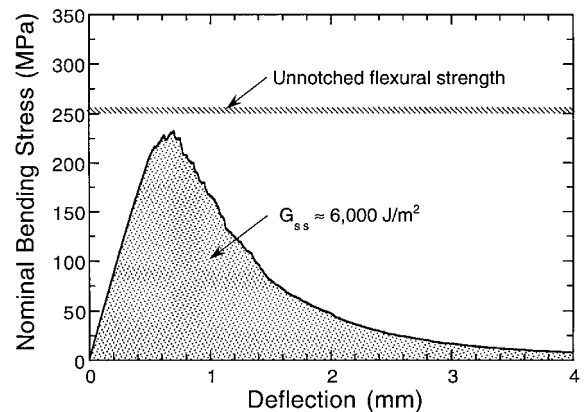


Fig. 10. Load-deflection response of a single edge-notched bend specimen, indicative of stable crack growth (notch length,  $a = 6$  mm, specimen width,  $W = 12$  mm). (Adapted from [21]).

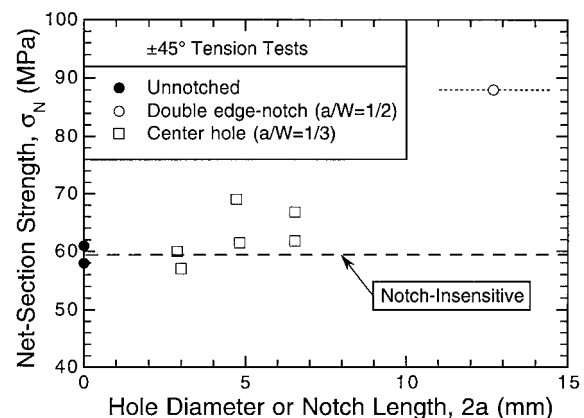


Fig. 11. Notch sensitivity in  $\pm 45^\circ$  orientation. (Adapted from [21]).

(Fig. 11).<sup>[21]</sup> Indeed, there appears to be some evidence of notch strengthening at the larger diameters, by ~10%. Failure occurs through a localization process closely analogous to that in the un-notched tension tests, with minimal fiber failure. Furthermore, the local strains at the hole edges at the load maximum reach values of 0.7–0.8%, ~2 to 3 times the failure strain measured in uniaxial tension.<sup>[21]</sup> Evidently the constraints associated with the hole suppress the onset of localization within the most heavily stressed regions (immediately ahead of the hole), resulting in the observed notch insensitivity. In the presence of long, relatively sharp notches, a transition in failure mechanisms occurs, to one involving fiber fracture (Fig. 12).<sup>[13]</sup> The corresponding strengths are increased substantially, by ~50% over the values obtained in both the un-notched and the center-hole specimens (Fig. 11). The observed notch “strengthening” appears to be unique to the porous matrix CFCCs, in part because of the relatively low values of strength obtained under matrix-dominated loadings (in the absence of notches) relative to the fiber bundle strength.

## 6. Long-Term Stability

The long-term performance of porous matrix CFCCs at the targeted service temperatures (~1000–1200 °C) is dictated by the stability of the microstructures of both the fibers and the matrix. In the fibers, strength degradation results from grain growth. In the matrix, degradation involves sintering, subject to the constraints imposed by the dense fibers, leading to a loss in damage tolerance. Furthermore, the degradation in fiber strength may increase the requirements on the allowable matrix properties to enable damage tolerance, thereby reducing composite toughness, potentially with little or no change in the matrix microstructure. These synergistic degradation mechanisms have yet to be quantified.

Fibers comprised of pure alumina (e.g., Nextel 610) are particularly susceptible to grain growth and strength reduction at temperatures ≥1000 °C. The problem is less severe in alumina-mullite fibers (e.g., Nextel 720) because of the constraint of the mullite on grain growth. Maintaining a stable matrix pore structure is an equally important and difficult challenge. Because of geometric considerations of infiltration and packing of matrix particles around the fibers, the matrix

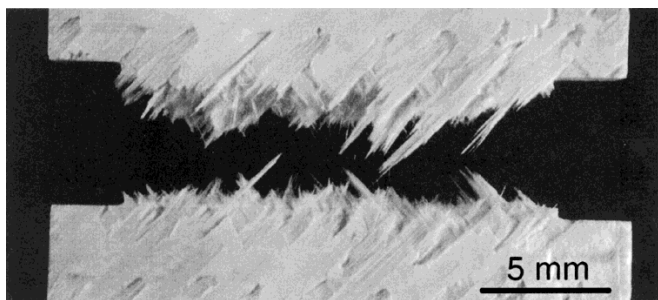


Fig. 12. Fiber failure in a notched porous-matrix CFCC specimen in the ±45° orientation [13].

particles are necessarily of a fine size scale, making them especially prone to subsequent sintering and densification. Indeed, the development of a pore structure that can be produced at moderate temperatures (to avoid fiber degradation) yet be retained over long periods at elevated temperatures remains one of the critical outstanding challenges in the development of porous matrix CFCCs.

Among the porous matrix CFCCs developed to date,<sup>[13,17,18]</sup> the one comprising the mullite–alumina matrix appears to exhibit the best potential for long-term stability. This stability has been demonstrated through measurement of retained strength following 1000 h exposures at elevated temperatures. Figure 13 shows the trends for two systems, both reinforced with Nextel 720 fibers, but with different matrices: alumina–silica<sup>[18]</sup> and mullite–alumina.<sup>[28]</sup> Strength degradation occurs in the former system at temperatures ≥1000 °C. By contrast, there is virtually no strength reduction in the latter system up to 1200 °C. Furthermore, the fracture surfaces of the mullite/alumina matrix system exhibit the desired fibrous appearance,<sup>[28]</sup> consistent with high damage tolerance, whereas the alumina–silica system fails in a brittle planar manner.<sup>[18]</sup> Despite the absence of strength reduction in the mullite–alumina system, there is some evidence of sintering, as manifest in elevations in the matrix hardness as well as increases in the opening displacement of the processing-induced cracks.<sup>[28]</sup> However, the magnitude of these changes is insufficient to degrade the fiber bundle strength over the 1000 h period, making the material an attractive candidate for some gas turbine applications requiring durability over extended time periods. Nevertheless, it is anticipated that yet longer exposures eventually will eventually lead to some loss in damage tolerance, analogous to that in the alumina–silica system. The time scale associated with this degradation remains to be established.

## 7. Concluding Remarks

Work to date has demonstrated the significant promise of the porous-matrix approach in enabling damage tolerance in

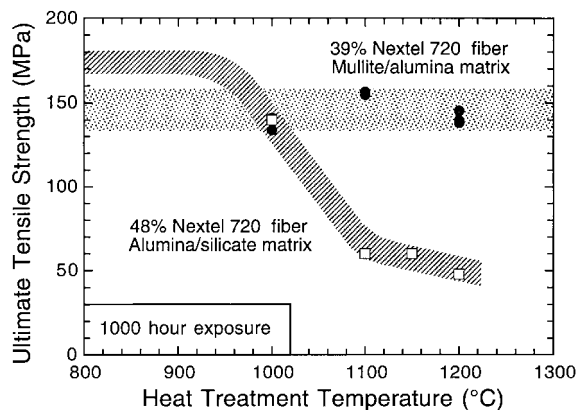


Fig. 13. Effects of matrix composition on the retained (room temperature) strength of porous matrix CFCCs reinforced with Nextel 720 fibers following high temperature exposures in air [18,28].

ceramic matrix composites, comparable to that resulting from the use of fiber coatings. Coupled with compositions based on all-oxide constituents, this approach offers an excellent opportunity to produce affordable components that have the requisite durability for long-term applications in energy-conversion systems. While the behavior of these materials is still not well understood, attributes such as their relative notch insensitivity make them attractive for incorporation into a design environment that is still largely dominated by practices evolved from the use of metals.

The primary drawback of these materials at the present time is an inadequate creep strength, owing primarily to the limited high temperature properties of available oxide fibers. As the properties of oxide fibers improve, the basic porous-matrix design should be extendable in principle to higher temperatures. Matrix compositions with the requisite characteristics to provide stability in the porous microstructure are likely to be similar to those used for the more advanced fibers, and hence compatible with them. Additional issues arise from the porous microstructure itself, which may have to be impervious to gas flow for some applications, or render the composite susceptible to penetration by moisture or contaminants. An interesting challenge is to make the composite impermeable, which would imply partially sealing and/or breaking the continuity of the porosity, without impairing its damage tolerance. These problems are currently under investigation.

Received: April 12, 2000  
Final version: July 19, 2000

- 
- [1] A. G. Evans, F. W. Zok, J. B. Davis, *Compos. Sci. Technol.* **1991**, 42, 3.
- [2] J. B. Davis, J. P. A. Löfvander, A. G. Evans, *J. Am. Ceram. Soc.* **1993**, 76, 1249.
- [3] T. J. Mackin, J. Y. Yang, C. G. Levi, A. G. Evans, *Mater. Sci. Eng. A* **1993**, 161, 285.
- [4] P. E. D. Morgan, D. B. Marshall, *J. Am. Ceram. Soc.* **1995**, 78, 1553, also **1995**, 78, 2574.
- [5] S. M. Johnson, Y. Blum, C. Kanazawa, H.-J. Wu, J. R. Porter, P. E. D. Morgan, D. B. Marshall, D. Wilson, *Key Eng. Mater.* **1997**, 127–131, 231.
- [6] D. B. Marshall, J. B. Davis, P. E. D. Morgan, J. R. Porter, *Key Eng. Mater.* **1997**, 127–131, 27.
- [7] R. W. Goettler, S. Sambasivan, V. Dravid, *Ceram. Eng. Sci. Proc.* **1997**, 18, 279.
- [8] M. K. Cinibulk, R. S. Hay, *J. Am. Ceram. Soc.* **1996**, 79, 1233.
- [9] M. G. Cain, R. L. Cain, M. H. Lewis, *J. Am. Ceram. Soc.* **1997**, 80, 1873.
- [10] M. Mattoni, J. Y. Yang, C. G. Levi, F. W. Zok, submitted to *J. Am. Ceram. Soc.*
- [11] M. Y. He, J. W. Hutchinson, *Int. J. Solids Struct.* **1989**, 25, 1053.
- [12] D. C. C. Lam, F. F. Lange, A. G. Evans, *J. Am. Ceram. Soc.* **1994**, 77, 2113.
- [13] C. G. Levi, J. Y. Yang, B. J. Dalgleish, F. W. Zok, A. G. Evans, *J. Am. Ceram. Soc.* **1998**, 81, 2077.
- [14] C. G. Levi, F. W. Zok, J.-Y. Yang, M. Mattoni, J. P. A. Löfvander, *Z. Metallkd.* **1999**, 90, 1037.
- [15] W. A. Curtin, *J. Amer. Ceram. Soc.* **1991**, 74, 2837.
- [16] M. Ibnabdeljalil, W. A. Curtin, *Int. J. Solids Struct.* **1997**, 34, 2649.
- [17] L. P. Zawada, *Ceram. Eng. Sci. Proc.* **1998**, 19, 327.
- [18] R. Jurf, S. Butner, *Proc. Int. Gas Turbine and Aeroengine Congress and Exhibition*, Indianapolis, IN **1999**.
- [19] V. Kramb, R. John, L. P. Zawada, *J. Am. Ceram. Soc.* **1999**, 82, 3087.
- [20] L. P. Zawada, R. S. Hay, S. S. Lee, J. Staehler, submitted to *J. Am. Ceram. Soc.*
- [21] J. A. Heathcote, X.-Y. Gong, J. Yang, U. Ramamurty, F. W. Zok, *J. Am. Ceram. Soc.* **1999**, 82, 2721.
- [22] F. F. Lange, W. C. Tu, A. G. Evans, *Mater. Sci. Eng. A* **1995**, 195, 145.
- [23] J. Haslam, K. E. Berroth, F. F. Lange, *J. Eur. Ceram. Soc.* **2000**, 20, 607.
- [24] F. Heredia, S. M. Spearing, T. J. Mackin, M. Y. He, A. G. Evans, *J. Am. Ceram. Soc.* **1994**, 77, 2817.
- [25] K. R. Turner, J. S. Speck, A. G. Evans, *J. Am. Ceram. Soc.* **1995**, 78, 1841.
- [26] T. J. Mackin, M. C. Roberts, *J. Am. Ceram. Soc.* **2000**, 83, 227.
- [27] J. C. McNulty, F. W. Zok, G. M. Genin, A. G. Evans, *J. Am. Ceram. Soc.* **1999**, 82, 1217.
- [28] E. Carelli, H. Fujita, J.-Y. Yang, F. W. Zok, submitted to *J. Am. Ceram. Soc.*
-